JOTCS A
Journal of the Turkish Chemical Society
Section: A
Chemistry
TURKISH CHEMICAL SOCIETY

Synthesis, characterization and antibacterial study of Co(II) and Cu(II) complexes of mixed ligands of piperaquine and diclofenac

Yusuf Oloruntoyin Ayipo[1,2*], Wahab Adesina Osunniran[2], Umar Muhammad Badeggi[3], Ismaila Olalekan Saheed[2], Akeem Adebayo Jimoh[2], Halimah Funmilayo Babamale[4], Emmanuel Olawuyi Olaide[2]

[1] Center for Drug Research, Universiti Sains Malaysia, 11800, Pulau Pinang, Malaysia.
[2] Department of Chemical, Geological and Physical Sciences, Kwara State University, Malete, P. M. B. 1530, Ilorin, Nigeria.
[3] Department of Chemistry, Cape Pennisula University of Technology, Cape Town, South Africa.
[4] Department of Chemistry, University of Ilorin, P. M. B. 1515, Ilorin, Nigeria.

Abstract: Pathogenic microorganisms develop incessant resistance toward antibiotics through various cellular defense mechanisms, thereby creating a search for chemotherapeutic alternatives, the potentials of which metal complexes of small-molecule drugs offer. In this study, Cu(II) and Co(II) complexes of mixed piperaquine and diclofenac were synthesized and characterized *via* magnetic moment determination, elemental analysis, FTIR, UV-Visible, 1D ^{1}H NMR, ^{13}C NMR spectroscopy and powder XRD, then evaluated for biological activities *in silico* and *in vitro*. The results provide evidence of coordination of the metal ions to ligands through N, COO and Cl groups with proposed octahedral geometry, low spin, paramagnetic, polycrystalline complexes. The physicochemical and pharmacokinetic parameters predicted *in silico* support bio-functionality and safety of the complexes. The complexes demonstrate strong inhibition against bacterial strains especially *Staphylococcus aureus in vitro*. Specifically, Cu(II) complex at 1% *w/w* inhibited a zone of 100 mm which is in multi-folds of the effects of piperaquine and diclofenac with 32 and 25 mm respectively, and better than ciprofloxacin with 92 mm. On DPPH assay, both complexes display better antioxidant potentials with respective IC_{50} of 165.09 and 382.7 µg/mL compared to ascorbic acid with 7526 µg/mL. Thus, the complexes represent therapeutic models for overcoming antibacterial resistance upon further study.

Keywords: Antibiotic resistance, bioinorganic, spectroscopy, powder XRD, biological study.

Submitted: March 18, 2021**. Accepted:** May 02, 2021**.**

Cite this: Ayipo Y, Osunniran W, Badeggi U, Saheed I, Jimoh A, Babamale H, et al. Synthesis, characterization and antibacterial study of Co(II) and Cu(II) complexes of mixed ligands of piperaquine and diclofenac. JOTCSA. 2021;8(2):633–50.

DOI: https://doi.org/10.18596/jotcsa.898523.

***Corresponding author. E-mail:** yusuf.ayipo@kwasu.edu.ng.

INTRODUCTION

Coordination chemistry between transition metal ions and various bioactive organic ligands have been employed to prepare several metal-organic chemical frameworks with enhanced pharmacological properties than the parent ligands. Upon coordination to metal ions, the systematic bioavailability, solubility, inertness for substitution, planar biocompatibility and other pharmaceutical profiles of the ligands become enhanced as well as the lipophilicity of the metal ions (1–3). The interesting medicinal profiles of these metal-based biomaterials stimulate the innovative design of various complex analogues for biological applications. A number of these hybrids are already approved or in clinical trials as anticancer/anti-pathogenic chemotherapeutics. Notably, the platinum-based anticancer drugs, Ga-68- and In-111-based complexes for radioimaging,

radiolabeling and therapy, gold-based Auranofin for treating rheumatoid arthritis, bismuth(III) ion-inclined bis(maltolato)oxovanadium(IV) with enhanced bioavailability and ability to reduce blood glucose in a clinical trial of diabetes, bismuth subcitrate and bismuth subsalicitrate (Pepto-Bismol) for treating peptic ulcers (4,5). Due to its coordination-induced action on bile acids and the disruption of charged cell walls of bacteria, the latter was proposed for further medicinal applications as an antacid and antibacterial agent. Some other new Bi(III)-containing bioactive complexes are continually under evaluation for antifungal, anticancer and antibacterial applicability (4).

Pathogenic microorganisms, especially bacteria, rapidly develop several defense mechanisms against antibiotics. These include the formation of biofilm, cell wall, encase efflux pumps, regulation of genetic and other intracellular materials (6). The intensive application of antibiotics over a long period and frequent exposure to non-lethal concentration also contribute to the incessant resistance of bacteria towards small-molecule drugs with specifically "bullet target" mode of action, which has, in turn, poses a great threat to the global healthcare (7), and thereby make a search for innovative therapeutic designs to overcome these healthcare challenge becomes imperative. Consequently, several conjugates involving antimalarial and antimicrobial ligands have been designed with improved combinatorial pharmacology (8). However, metal complex polymers inclusively exhibit a multi-target mechanism that favours several cellular processes, leading to their pleiotropic effects on the drug-resistant bacterial cells, thus become promising agents under the United Nation (UN) sustainable developmental goal 3.3 for prevention and treatment of communicable diseases (9). Some of these agents have been designed using organic small-drug molecules such as sulfadoxine, sulfisoxazole, quinazoline, pyrimethamine, quinoline, pyrazolone, phenylhydrazine etc with improved pharmacological profiles due to favourable pharmacophoric moieties of ligands (singly/mixed) in coordination to metal ions such as Co(II), Cu(II), Mn(II), and Zn(II) (10–15). However, none has been reported of mixed ligands involving piperaquine (Pip) and sodium diclofenac (NaD). In our previous studies, we have demonstrated impressive antioxidant and bactericidal activities of Cu(II), Zn(II), and Co(II) complexes consisting of piperaquine, acetaminophen and acetylsalicylic acid as mixed ligands (16).

Therefore, this study aims at the preparation of coordination compounds consisting of Co(II) and Cu(II) ions in complex with sodium NaD and Pip as mixed ligands using solvent-based inorganic synthetic approach, characterization and evaluation of antioxidant and antibacterial activity *in vitro* as well as some *in silico* biological studies, while adopting some reported protocols (10,14–18) with modifications.

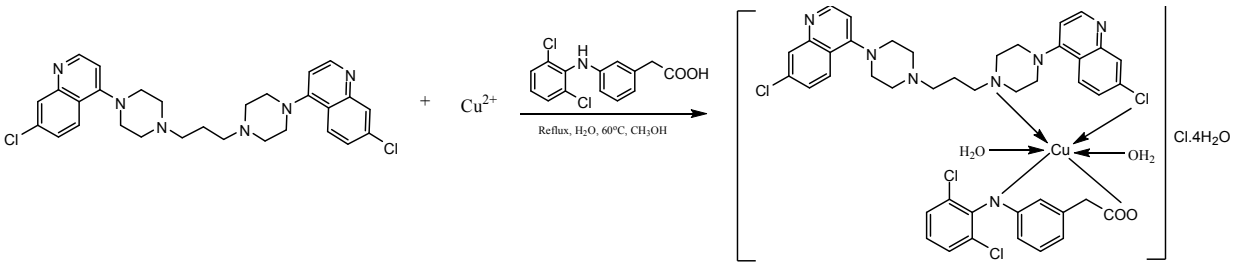
MATERIALS AND METHOD

Materials

The materials were used as commercially obtained without further purification. These include copper(II) chloride hexahydrate ($CuCl_2.6H_2O$), cobalt(II) chloride hexahydrate ($CoCl_2.6H_2O$), distilled H_2O, ethanol, methanol, acetone, dimethyl sulfoxide (DMSO), lactic acid, acetic anhydride, and silica gel-coated thin layer chromatographic (TLC) plate from Sigma Aldrich, England. The ligands, Pip and NaD were obtained from Zhuhai Rundu Pharmaceuticals, China and Tuyil Pharmaceutical, Nigeria, respectively.

Synthesis of Copper(II) Complex of Mixed Piperaquine and Diclofenac

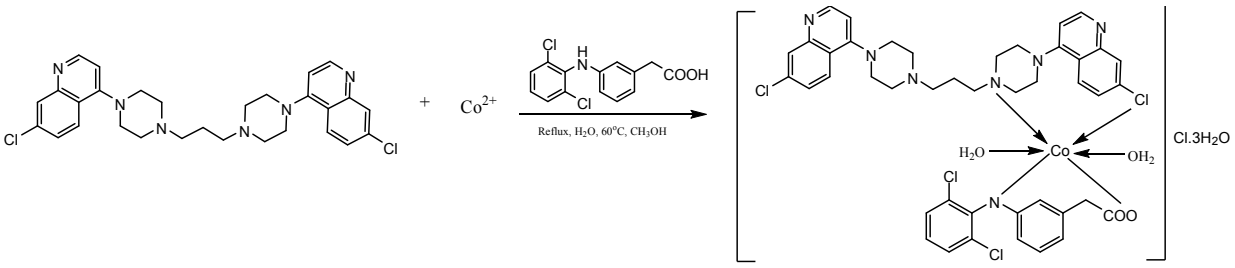
The Cu(II) complex of mixed Pip and NaD ligands was prepared by reacting a 0.002 mol of $CuCl_2.6H_2O$ previously dissolved in 20 mL of distilled H_2O with 0.002 mol Pip in 20 of mL hot distilled water and subsequently adding a solution containing 0.002 mol NaD in 20 mL of methanol. The mixture was refluxed for 2 hours and 30 minutes after which the resulting stable precipitates formed (Scheme 1) were filtered, washed with hot water, then cold water twice to remove unreacted ligands and kept in a desiccator with $CaSO_4$ for 24 hours. The progress of the reaction was monitored using TLC. Yield: 3.62 g (38%); M.P. 231 – 232 $^{\circ}$C; UV (DMSO) λ_{max} (nm): 248, 342, 704; FTIR (KBr) ν_{max} (cm^{-1}) 3323 (H_2O), 1592 $(COO)_{asy}$, 1380 $(COO)_{sym}$, 741, 662 (CCl), 504, 562 (Cu-O/N); ^{1}H NMR (d_6-DMSO, 400 MHz) 6.27 (d, J = 7.2 Hz), 6.86 (d), 7.05 (d), 7.18 (d), 7.51 (d, 8.4 Hz), 7.66 (d, J= 9.6 Hz), 8.21(br, s), 3.45 (br), 3.21 (br), 3.16 (s), 2.06 (br, s), 3.91(br), 1.20 (s) ppm. ^{13}C-NMR (d_6-DMSO, ~100 MHz) 49.1, 49.4, 51.4, 53.7, 116.4, 121.3, 124.4, 126.1, 127.1, 128.1, 129.6, 130.4, 131.4, 137.5, 143.1 ppm. Anal. Calcd. Mass fractions of elements, w/%, for $C_{43}H_{53}Cl_6CuN_7O_8$ (M_r = 1073) are C 48.17, H 4.98, Cu 5.93, N 9.14; Found: C 47.21, H 5.35, Cu 6.14, N 9.80.



Scheme 1: Proposed reaction pattern between mixed piperaquine/diclofenac and Cu(II) ion.

Synthesis of Cobalt(II) Complex of Mixed Piperaquine and Diclofenac

The Co(II) complex of mixed Pip and NaD was synthesized by refluxing 0.002 mol of NaD previously dissolved in 20 mL methanol with 0.002 mol of Pip dissolved in 20 mL hot water and 0.002 mol of $CoCl_2.6H_2O$ under constant stirring for 5 hours and 30 minutes after which a stable pink precipitate was formed (Scheme 2). The precipitates were filtered, washed with hot water, then twice with cold water and dried in a desiccator for 24 hours. The progress of the reaction was monitored using TLC. Yield: 4.12 g (47%); M.P. 230 – 234 °C; UV (DMSO) λ_{max} (nm): 232, 450, 662; IR (KBr) ∇_{max} (cm^{-1}) 3323 (H_2O), 1590 $(COO)_{asy}$, 1380 $(COO)_{sym}$, 741, 662 (CCl), 520, 574 (Co-O/N); ^1H NMR (d_6-DMSO, 400 MHz) 2.07 (s), 3.17 (s), 3.71 (s), 6.28 (d, J= 8.4Hz), 6.86 (t), 7.06 (t), 7.16 (s), 7.19 (d, J=8.0Hz), 7.50 (d, J-=8.00Hz), 7.20 (d, J=8.8 Hz) ppm. ^{13}C-NMR (d_6-DMSO, ~100 MHz) 49.3, 116.5, 121.5, 125.9, 128.2, 129.8, 130.4, 131.5, 137.5, 143.2. Q= 125.9, 130.4, 139.5, 143.2 ppm. Anal. Calcd. Mass fractions of elements, w/%, for $C_{43}H_{51}Cl_6CoN_7O_7$ (M_r = 1050) are C 49.21, H 4.90, Co 5.62, N 9.34; Found: C 48.16, H 4.85, Co 5.81, N 9.48.



Scheme 2: Proposed reaction pattern between mixed piperaquine/diclofenac and Co(II) ion.

Characterization

The melting point of the synthesized complexes was recorded on a Gallenkamp melting point apparatus. Solubility tests of the ligands and the complexes were carried out using acetone, dilute lactic acid, distilled water, methanol and dimethyl sulfoxide while the ionic properties of the ligands and their corresponding metal complexes were measured using a conductivity meter CDM 210, MeterLab model. The functional groups in the ligands and the complexes as well as the coordination-induced shifts in spectral bands were identified by loading their disc-powder on FTIR (Shimadzu, Japan) with a scan range of 400-4000 cm^{-1} wavenumber, resolution of 4 cm^{-1} using KBr pellets as blank. The electronic (UV-Visible) spectra of the complexes in solution were run in the range 190-900 nm on a Perkin Elmer *20λ* spectrophotometer with the samples placed in quartz cuvettes of 1 cm path length and DMSO was used as a blank. The magnetic susceptibility of the metal chelates was determined on a Gouy balance at room temperature using $Hg[Co(SCN)_4]$ with the corrections of diamagnetic on Pascal's constants.

Powder X-ray Diffraction Spectroscopy

D8 Advance diffractometer, with the measurement of continuous ∂-∂ scan in a locked coupled-mode having a tube of Cu-Kα radiation ($\lambda K\alpha_1$=1.5406Å) and detector of LynxEye (Position sensitive detector) was employed for the powder X-ray diffraction analysis at iThemba Scientific Lab., South Africa. The diffractograms were studied to identify the powdered-crystal structures and morphology of the complexes while the value for 2θ for Miller indices estimation was determined using the Bragg's law (Eq. 1) (19,20):

$$\lambda = 2 d_{hkl} \sin\theta \qquad \text{(Eq. 1)}$$

Where λ = X-ray wavelength (Cu = 1.5406 Å), d = interplanar distance and θ = diffraction angle.

The crystalline domain sizes indicated by the broadening of the peak especially when the sizes of the crystal become small were estimated theoretically using the Scherrer equation (Eq. 2) (21):

$$D = \frac{k\lambda}{\beta \cos\theta} \quad \text{(Eq. 2)}$$

Where D = crystalline domain size, k = Scherrer constant usually given as 0.9 and β = peak width at half of its height

^{1}H NMR, ^{13}C NMR and DEPT-135 NMR Spectroscopy

The Nuclear magnetic resonance (NMR) spectroscopy NMR spectra of the complexes were recorded at 25 °C on a Bruker Avance 400 MHz NMR spectrometer (Germany), with deuterated Dimethyl sulfoxide (DMSO) used as a solvent. Chemical shifts of ^{1}H (δH) and ^{13}C (δC) and DEPT (δC) were determined in ppm, relative to tetramethylsilane as reference.

Elemental Analyses

The percentage by mass of some major elements in the complexes such as C, H, N and Cu/Co (M) was determined using the Vario El Cube Elemental Analyzer at the Central Analytical Facilities, Stellenbosch University, South Africa.

Preliminary Test for Water Molecule and Chloride Ion

The presence of water of crystallization within or outside the coordination sphere of each complex was assessed using cobalt chloride paper. The color change of the paper from blue to pink indicates positive test. For the chloride ion outside the coordination sphere, aqueous $AgNO_3$ and NH_4OH were used for confirmation on the solution of each complex while a white precipitate soluble in excess NH_4OH indicate the presence of uncoordinated Cl^- ion.

Determination of Water of Crystallization

The presence of some water of crystallization in the complexes is confirmed by heating the sample to a constant weight, testing the gas evolved with cobalt(II) chloride paper, anhydrous copper (II) sulfate. The amount of water of crystallization was determined using the Eq. 3 below.

$$\frac{\text{mass of anhydrous complex}}{\text{molecular mass of anhydrous complex}} = \frac{\text{mass of hydrated complex}}{\text{molecular mass of hydrated complex}} \quad \text{(Eq. 3)}$$

Biological activity

In silico predictions of biological activity and ADMET properties

The broad spectrum of biological activities resulting from the interactions of the synthesized complexes with various enzymes/proteins responsible for bio-functions was predicted using the cheminformatics and bioinformatics interface of Molinspiration server (https://molinspiration.com/cgi-bin/properties) by the input of SMILES file in each case. The Java tools incorporated within the server supports computational analysis through the algorithm of active training sets generation from which the cumulative bioactivity of the target molecules is predicted through probable fragments. Each sample was scored for likeliness in activity through various inhibition mechanisms on G protein-coupled receptor (GPCR), kinase, nuclear receptor, and enzyme as well as ability to modulate ion channel.

The physicochemical and pharmacokinetics profiles of the complexes were predicted in terms of adsorption, distribution, metabolism, excretion and toxicity (ADMET) using the web-based Swiss ADME computational tools by inputting the SMILES file of each complex (17,22). The properties further reveal the drug-likeness of the molecules under study.

Antioxidant properties

The sample of each complex and the standard, ascorbic acid was weighed into the sample bottle, 9 mL of the solvent was added to each sample to make a solution of 100, 200, 300, 400 and 500 µg/mL. Each solution was then partitioned into three (3 mL each) for triplicate tests and transferred into the test tube. A 0.0039 g of DPPH was weighed into a reagent bottle and 100 mL of the ethanol was added and 3 mL of DPPH solution was added into each test tube containing the test sample. The setup in test tubes was kept in a dark room for thirty minutes after which absorbance was read at 517 nm wavelength. The IC_{50}, which stands for the concentration of fraction required for 50% scavenging activity, was calculated from the dose-inhibition linear regression equation (eqn. 4) for each complex.

$$\%\text{inhibition} = \frac{(\text{Abs}_{control} - \text{Abs}_{sample})}{\text{Abs}_{control}} \times 100 \quad (4)$$

Antibacterial Screening

The solutions of the ligands and the synthesized complexes were tested against strains of some gram-positive and gram-negative bacteria, *Pneumonia aeruginosa, Escherichia coli* and *Staphylococcus aureus* to determine and compare their potential bactericidal activities by measuring their inhibition zones around the inoculated organism wells, adopting agar dilution techniques as well as the standard recommendation of Clinical and Laboratory Standards Institute, 29th Edition (16,23).

RESULTS AND DISCUSSION

Some physicochemical properties such as solubility, melting point, and color of the ligands and the corresponding metal complexes are presented in Table 1. The complexes, ligands and metal salts

were mostly insoluble in organic solvents of acetone and methanol but all are soluble in DMSO, possibly due to its high polarity and donor strength (14) which enhance its ionic interaction with the samples in solution. The ionic nature of the complexes as shown by the conductivity results could be traced to the presence of electropositive metal ions in their structures compared to the parent ligands. The melting points of the complexes are lower when compared to the salts/ligands and the sharpness could imply a good purity of the complexes (24). The significant changes in the melting points, as well as colors between the ligands and their respective metal complexes, indicate a change in the atomic structures, possibly due to chemical coordination. Invariably, this could affect new electronic transitions and the ligand-metal lattice structures (12,25) as we observed in the subsequent characterization results.

The Infra-Red spectroscopy data of the ligands and the metal complexes are presented in Table 2, Figures 1 & 2. The spectra of the ligands and metal complexes were studied and compared to identify the mode and sites of metal-ligand chelation. The band at 3259 cm^{-1} which could be assigned to the N-H group of NaD ligand disappeared in the two complexes. Similarly, the stretching bands at 3286 and 3433 cm^{-1} attributable to the two asymmetric piperazinyl and imine N-groups of the Pip ligand have significantly undergone bathochromic and hypsochromic shifts respectively in the complexes, indicating the possibility of their participation in coordination. More so, the spectral bands of 1398 and 1575 cm^{-1} which are assignable to the symmetric and asymmetric COO group in the NaD ligand have shifted to a higher and lower wavenumber of 1592/1590 and 1380/1380 in the Cu(II) and Co(II) complexes respectively with a significant difference. The difference in the asymmetric and symmetric stretching vibration of the COO groups, $\Delta = \nu(COO)_{asy} - \nu(COO)_{sym}$ gave a value of 212 and 210 cm^{-1} for Cu(II) and Co(II) complex respectively, indicating the contribution of the COO of NaD to coordination as a monodentate ligand (15) with the Δ value of 177 cm^{-1} which agrees with the ionic value of NaD. These also support the possibility of bidentate-chelation between NaD to both Cu(II) and Co(II) ions through the NH and COO (25,26). In a similar pattern, Pip, a nitrogen-based ligand, shows coordination to the metal ions through the amine N and the Cl as evidenced by the disappearance of the band 3286 cm^{-1} attributable to the amine N with Δ value of 147 cm^{-1}, and also the hypsochromic shift of C-Cl band at 650 cm^{-1} in the ligand to 662 cm^{-1} in the metal complexes, indicating the possibility of coordination through the Cl group. These rationally suggest the ligand to act as a bidentate ligand (16). The complexes show weak/medium bands in the range 504 – 662 cm^{-1} which are tentatively assigned to M-N/O/Cl stretching vibrations and also contributing to the evidence of coordination. The spectra bands at 3433 and 3323 in both ligands and the complexes indicate H_2O-metal chelation (Figures 1 & 2) (27).

Table 2: Major IR bands of the ligands and their complexes.

Ligands/ Complexes	**ν (NH)asy (NH)sym cm^{1-}**	**δ (NH) cm^{1-}**	**ν (COO)asy (COO)sym cm^{1-}**	**ν (CCl) cm^{-1}**	**Δ cm^{-1}**	**ν (MO/N) cm^{-1}**
NaD	3259	1507	1575 1398	747	177	--
Pip	3433 3286	1503	-	650	147	-
[Cu(NaD)(Pip)]	3323	1506	1592 1380	741 662	212	504, 562 614
[Co(NaD)(Pip)]	3323	1506	1590 1380	741 662	210 $_{for\ COO}$	520, 574, 611

Table 1: Some physicochemical parameters of the ligands and metal complexes.

Complexes/ Ligands/Metals	**Cond. ($\Omega^{-1}cm^{-1}$)**	**Solubility**						**M.P. (°C)**	**Color**
		D. H_20	LA	AES	DMSO	Me_2CO	MeOH		
NaD	-	NS	S	PS	S	PS	S	289-290°C	White
Pip	-	PS	S+Δ	PS	S	PS	NS	250-252°C	White
$CuCl_2.6H_2O$	ND	S	S	NS	S	NS	NS	486-490°C	Blue
$CoCl_2.6H_2O$	ND	S	S	S	S	S	NS	735-737°C	Brick Red
[Cu(NaD)(Pip)]	1.6×10^{-4}	PS+Δ	NS	PS+Δ	S	NS	S+Δ	231-232°C	Blue
[Co(Pip)(NaD)]	2.1×10^{-4}	NS	NS	NS	S	NS	PS+Δ	230-234°C	Brown

S = Soluble, NS = Not soluble, PS = Partially soluble, Δ =Heat, AES= Aqua ethanolic solution LA= Lactic acid, $D.H_2O$=Distilled water, DMSO= Dimethyl sulfoxide, MeOH = Methanol, Me_2CO = Acetone, ND = Not determined.

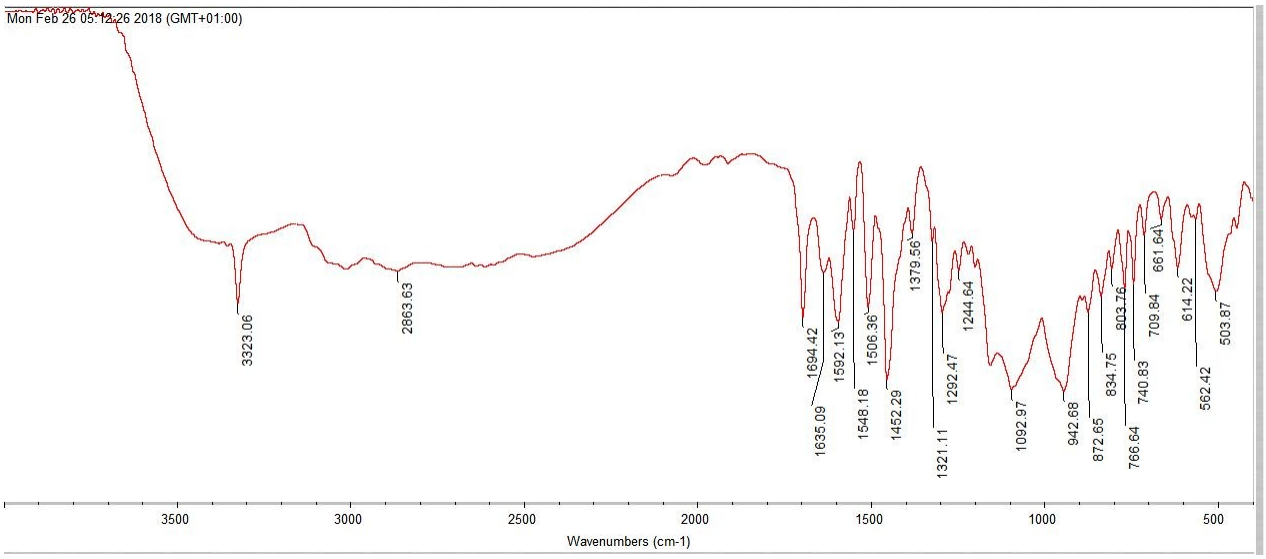


Figure 1: FTIR Image of [Cu(NaD)(Pip)].

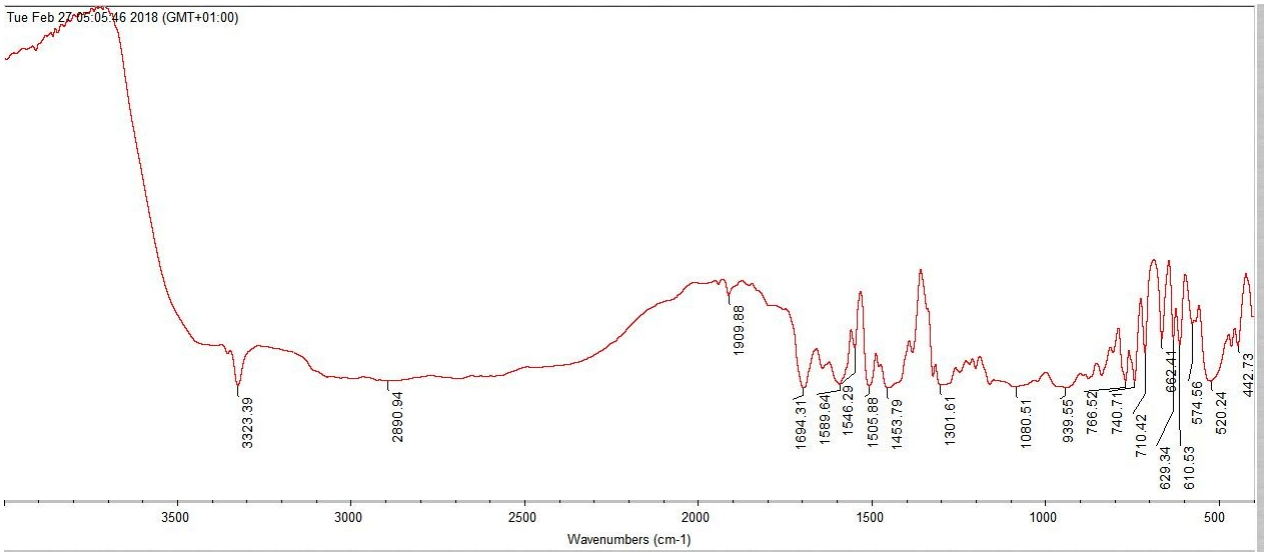


Figure 2: FTIR Image of [Co(NaD)(Pip)].

The electronic spectra, magnetic moment, and elemental analysis results of the synthesized metal complexes are reported in Table 3. The Cu(II) and Co(II) complexes have a low spin of d^9 and d^7 configurations respectively with the highest filled orbital as $^2t_{2g}$ (xy, xz, yz). Thus, the ground state is paramagnetic and labelled ^2E_g and $^4T_{1g}$ respectively. The electronic spectra of the ligands in DMSO exhibited transition at 202 nm – 379 nm which were assigned to intra-ligand transitions (n → σ*, n → π* and π → π*). The UV-Visible spectra of the [Cu(Pip)(NaD)] show a single broad absorption band at 704 nm assignable to $^2E_g \rightarrow {}^2T_{2g}$ transition, while [Co(Pip)(NaD)] had three bands within the visible region, 450, 539, and 662 nm assignable to $^4T_{1g}(F) \rightarrow {}^4T_{2g}(F)$, $^4T_{1g}(F) \rightarrow {}^4A_{2g}(F)$ and $^4T_{1g}(F) \rightarrow {}^4T_{1g}(P)$ transitions respectively, thus, suggesting the formation of octahedral geometry with hybridizations of sp^3d^2 and dsp^3d for [Cu(Pip)(NaD)] and [Co(Pip)(NaD)] respectively (17,28,29). The magnetic susceptibility measurement revealed that the Cu(II)- and Co(II)-containing complexes have effective magnetic moments of 1.53 and 1.47 B.M. respectively, further strengthening the octahedral geometry suggested for the complexes arising from their unpaired electrons (17,30,31). The presence of the ligands in the complexes as proposed (Schemes 1 & 2) was supported with good consistency between the CHNS elemental analysis results (Supplementary file) and the suggested molecular formulas.

The preliminary assay by heating indicates the presence of water of crystallization in the complexes when each sample was gently heated to a constant weight of 3.38 and 3.91 g for Cu(II) and Co(II) complex, respectively. This was further confirmed by testing the evolved gases with cobalt chloride paper which changed from blue to pink color. The estimates using Eq. 3 support the proposal of 4 and 3 molecules water of crystallization in one molecule of their respective complexes. Although, a more accurate analysis

such as the thermogravimetric analysis (TGA) is required for further confirmation. In a similar preliminary test, a white precipitate was observed upon the addition of aqueous $AgNO_3$ to the solution of each complex. The precipitates became dissolved when excess NH_4OH was added, tentatively indicating the presence of Cl^- outside the coordination sphere.

^{1}H NMR, ^{13}C NMR and DEPT-135 NMR Spectroscopy

The ^{1}HNMR spectrum (Figure 3A) of [Cu(Pip)(NaD)] whose formation was reported at the synthesis section (Scheme 1), was run in deuterated DMSO. From the NaD moiety, the signals at 8.21 and 3.45 ppm are both singlets and can be assigned to nitrogen proton between the aromatic rings and methylene proton situated between carbonyl carbon and aromatic ring which might have shifted them further upfield. In the aromatic region, the signals at 7.18 (s) and the doublet 7.66 ppm (d, J= 9.6 Hz) can be assigned to other unsubstituted benzene rings of the NaD ligand. The chemical shifts were rather downfield compared to neighboring benzene which is doubly substituted with chlorine atoms. On the Pip moiety, the chemical shifts at 6.27 ppm (d, J = 7.2 Hz) and 7.51 ppm (d, J = 8.4 Hz) could be rationally assigned to the unsubstituted benzene rings while the downfield signals at 1.20, 2.06, 3.16 and 3.21 ppm are assignable to the shielded CH_2 groups of the piperazinyl moieties. The ^{13}C-NMR (Figure 3B) in the same vein shows 21 carbon atoms as expected of both Pip and NaD in the aromatic carbons (116.1 - 143.1) ppm. However, the reduced intensities of signals at 49.1, 49.4, 51.5 and 53.7 ppm can be ascribed to the methylene of the two ligands contained in the aliphatic region. Thus, the two ligands are represented in the complex accordingly.

From the nuclear magnetic resonance spectroscopy values obtained for [Co(Pip)(NaD)] using DMSO, both ligands were adequately represented. More study of the NaD moiety (Scheme 2) reveals two conspicuous singlets at 3.17 and 3.71 ppm (Figure 3C), corresponding to the protons adjacent to the carbonyl carbon and the amino proton in between the benzene rings respectively. Downfield the aromatic region, the only singlet at 7.16 ppm is due to an aromatic proton adjacent to the chloro-substituted carbon in the Pip ring. Since there are four doublets overall, the more deshielded protons would be those close to the chlorine atom in the diclofenac moiety. This is because of the electron-withdrawing ability of chlorine atoms, thereby shifting the protons further downfield at 7.50 ppm. Similarly, the doublet on the chloro substituted ring on the Pip would also feel this effect and their neighborhood with chlorine. This has also caused the protons deshielded although not as the previous one. Therefore, the signal at 7.20 ppm can be reasonably assigned to them. Other signals at 7.19 and 6.25 ppm are assignable to the doublet of the remaining rings in Pip and NaD moiety respectively. Also, the triplets at 6.86 ppm and 7.06 ppm from the spectra can be unambiguously assigned to signals of the two rings of the NaD ligand. The difference in values is due to the proximity of protons to an electron-withdrawing entity (7.06 ppm) and others for electron donor substituents attach to the resonating rings.

The ^{13}C-NMR (Figure 3D) supports the above assignment and further corroborated by DEPT-135 values. When intensities of the signals are carefully observed, the total number of carbon atoms from the spectra matches the two ligands which further explain their involvement in the coordination. The DEPT-135 (Figures 3E & 3F) also revealed quaternary carbons between 130.4 – 143.2 ppm (15,25).

Some copper(II) complexes reported exhibit paramagnetism in relevance to their electronic configurations which allow a $d_{x^2-y^2} \rightarrow d_{xy}$ transition and this supports various biomedical applications including imaging, on-site delivery and antimicrobial effects (32). Suggestively, the broad, almost unreadable signals between 3.45 – 3.91 ppm and 3.17 – 3.89 ppm in Cu(II) and Co(II) complex, respectively (Figure 3A & 3C) could have rationally resulted from the effects of the unpaired electron spin exerted on the nuclear spin relaxation, depending strongly on the spatial distance of the paramagnetic centre to the nucleus and the nature of the paramagnetic center itself. The pseudo-contact shifts possibly induced by the interaction between nucleus spin and the magnetic dipole produced by the spinning of unpaired electrons. It could be suggested that the nucleus of atoms bond directly to the paramagnetic center (33,34) and further supports the argument for paramagnetic complex formation in both cases as previously proposed from the electronic configuration, possible hybridization, electronic transition and magnetic moments. The essential application mostly relevant to this study is their DNA cleaving ability peculiar to Cu(II) and Co(II) ions (35), which further supports the bactericidal activity of their complexes. Nonetheless, electron paramagnetic resonance (EPR) is necessarily required for further validation of this biologically important hypothesis.

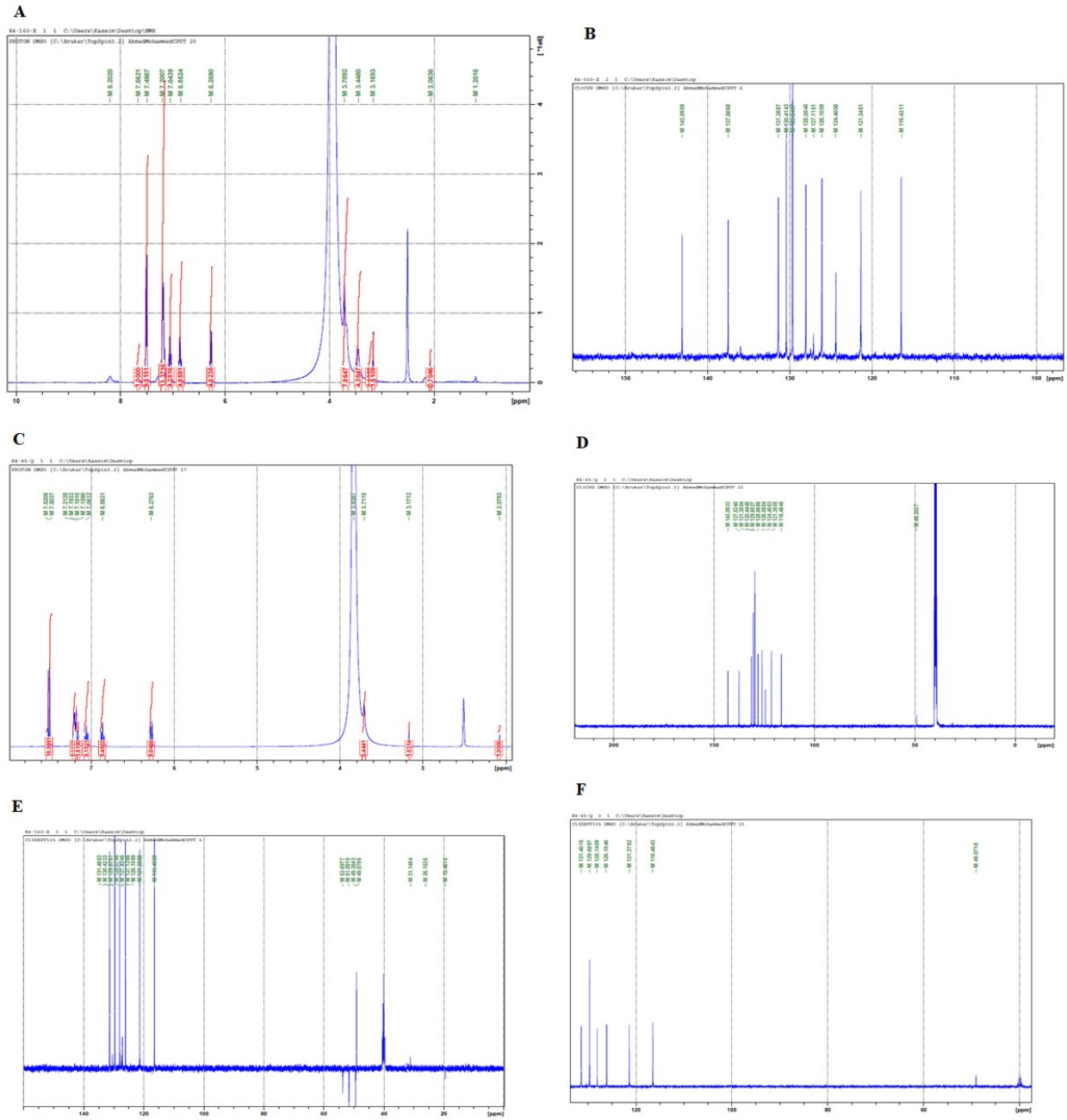


Figure 3: Nuclear magnetic spectra of the complexes (A) ^{1}H NMR of [Cu(Pip)(NaD)] (B) ^{13}C NMR of [Cu(Pip)(NaD)] (C) ^{1}H NMR of [Co(Pip)(NaD)] (D) ^{13}C NMR of [Co(Pip)(NaD)] (E) DEPT-135 NMR of [Cu(Pip)(NaD)] (F) DEPT-135 NMR of [Co(Pip)(NaD)]

Table 3: Results of Electronic Transition and Elemental Analysis.

Compounds	**λ_{max} (nm)**	**$\bar{\upsilon}$ (cm^{-1})**	**Transition**	**$\mu_{eff\ (B.M)}$**	**Elemental % Calculated (Found)**			
					C	**H**	**N**	**M**
NaD	270	42553	π → π*	-				
	364	25381	n → π*					
Pip	202	49505	n → σ*	-				
	379	26385	n → π*					
[Cu(Pip)(NaD)]	704	14205	$^2E_g \rightarrow {}^2T_{2g}$	1.53				5.93 (6.14)
	342	29240	n → π*					
	248	40323	π → π*		48.17 (47.21)	4.98 (5.35)	9.14 (9.80)	
[Co(Pip)(NaD)]	662	15106	$^4T_{1g}(F) \rightarrow {}^4T_{2g}(F)$	1.47				
	539	18553	$^4T_{1g}(F) \rightarrow {}^4A_{2g}(F)$					5.62 (5.81)
	450	22222	$^4T_{1g}(F) \rightarrow {}^4T_{1g}(P)$					
	232	43103	n → π*		49.21 (48.16)	4.90 (4.85)	9.34 (9.48)	

Powder X-ray Diffraction

The XRD data presented in Tables 4 & 5 revealed the diffraction patterns of the complexes, the estimated Miller indexing (hkl) and the crystal structures by mathematical method (36). The interplanar distances, "d" was determined using Bragg's equation (Eq. 1). The diffractograms indicate that the two complexes are polycrystallites in structure due to their peak profiles. The result data in Table 4 & 5 confirm some of the crystals as simple, body-centered, face-centered cubic and overall orthorhombic having conformed to the eqn. 5 & 6 (36–38):

$$\frac{1}{d^2}=\frac{h^2+k^2+l^2}{a^2} \qquad \text{(Eq. 5)}$$

for reflections cubic crystal and

$$\frac{1}{d^2}=\frac{h^2}{a^2}+\frac{k^2}{b^2}+\frac{l^2}{c^2} \qquad \text{(Eq. 6)}$$

for overall orthorhombic conformations (28,36).

The data also confirmed the novelty of the complexes, i.e. different from those of the existing organic and inorganic compounds on the JCPDS files, as supporting evidence of new compounds. Also, the atomic lattice structure of the ligands and that of the metal salts (found in the existing JCPDS data files) have changed in the complexes possibly due to coordination. The sharp distinctive peaks in the diffractograms (Figures 4 & 5) further indicate good purity of the complexes, although, purer single crystals could not be obtained from the recrystallization process after several attempts.

Table 4: Miller indexing, interplanar distances and crystalline system of [Cu(Pip)(NaD)].

Peak No.	$h^2+k^2+l^2$	hkl	2θ obs.	2θ Cal.	d-sp obs.	d-sp cal.	Rel. I	Lattice
1	3	111	15.22	15.21	5.82	5.82	69	10.0856
2	4	200	18.82	18.55	4.78	4.71	78	9.4283
3	5	210	20.4	20.49	4.33	4.35	89	9.7203
4	8	220	24.41	25.06	3.55	3.64	97	10.3051
5	10	310	28.49	27.34	3.26	3.13	100	9.8952
6	12	222	30.04	28.68	3.11	2.97	78	10.2936
7	13	320	32.06	32.9	2.72	2.79	78	10.0547

Lattice Parameters: a = 10.09 Å, b = 9.43 Å, c = 9.72 Å, Average Lattice = 9.97 (Å); Cubic Crystals with Reflections in Simple, Face-centered and Body-centered.
Overall Orthorhombic, $a_1 \neq a_2 \neq a_3$; $\alpha = \beta = \gamma = 90^\circ$

Table 5: Miller indexing, interplanar distances and crystal system of [Co(Pip)(NaD)].

Peak No.	$h^2+k^2+l^2$	hkl	2θ obsd.	2θ Calcd.	d-sp obsd.	d-sp calcd.	Rel. I	Lattice
1	3	111	10.73	10.73	8.24	8.24	92	14.3041
2	6	211	15.26	15.21	5.82	5.8	95	14.2226
3	9	300, 221	18.93	18.83	4.71	4.68	80	14.0637
4	11	311	20.54	20.4	4.35	4.32	90	14.3266
5	16	400	24.44	24.71	3.6	3.64	98	14.5573
6	21	421	28.53	27.77	3.21	3.13	100	14.3277

Lattice Parameters: a = 14.30 Å, b = 14.22 Å, c = 14.06 Å, Average Lattice = 14.30 (Å); Cubic Crystals with Reflections in Simple, Face-centered and Body-centered.
Overall Orthorhombic, $a_1 \neq a_2 \neq a_3$; $\alpha = \beta = \gamma = 90^\circ$

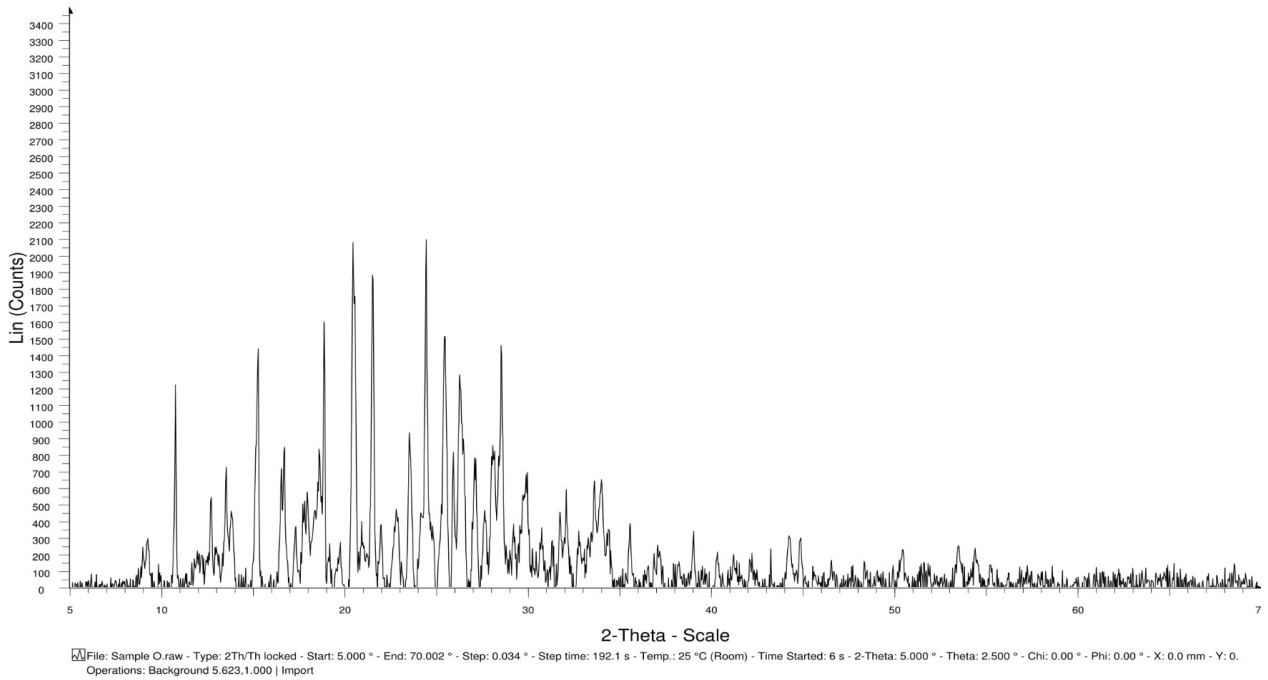


Figure 4: X-ray Diffraction Pattern of [Cu(Pip)(NaD)].

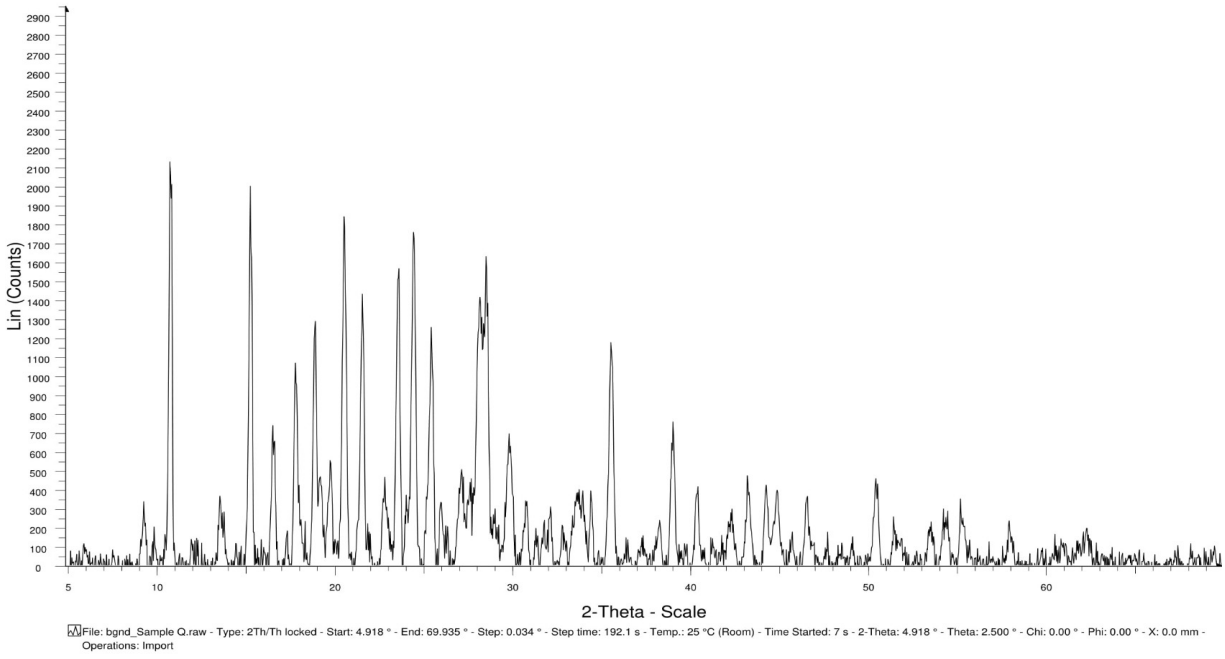


Figure 5: X-ray Diffraction Pattern of [Co(Pip)(NaD)]

Water of Crystallization

In addition to the positive result obtained for the presence of molecules of water of crystallization in the complexes using preliminary chloride paper test, the amount of the water molecules in each complex was determined using thermal analysis (Eq. 3). When 1.00 g of each for Cu(II) and Co(II) complexes with respective estimated molecular weights of 1073 and 1050 were subjected to heating gently. The weight continuously reduced until it

became constant at 0.93 and 0.95 g, respectively. Using Eq. 3, the water of crystallization was deduced as 4.19 (≈4) and 2.91 (≈3) for Cu(II) and Co(II) complex, respectively. These values together with other characterization data were used to propose the structure of the complexes in the absence of single crystals.

Biological Study

In silico predictions of biological activity and ADMET properties

The bioactivity profiles of the complexes are predicted *in silico* in comparison with the parent ligands, Pip and NaD to observe the possibility of enhanced interaction with biological targets and pharmacology due to coordination (Table 6). These interactions with major targets for essential biofunctionalities such as the GPCR, ion channel, kinases, nuclear receptor, protease and enzymes are evaluated in terms of binding affinity. All the complexes virtually demonstrate higher binding affinity against the receptors than the parent Pip and NaD as indicated by lower binding scores (especially the more negative ones). Although the geometric structures of the complexes are larger than the respective ligands, however, the enhanced binding affinity to the receptor as deduced for the complexes could be due to additive interactions of the metal ions and stabilization to the protein structures which sometimes naturally contain Cu(II) and Co(II) as cofactors (39). The theoretical interactions with these targets further predict their applicability as bioactive agents and promising bioactivity (17).

Table 6: Predicted bioactivity profile of the ligands and their complexes.

Compound	GPCR Ligand	Ion Channel Modulator	Kinase Inhibitor	Nuclear Receptor Ligand	Protease Inhibitor	Enzyme Inhibitor
Pip	0.22	0.12	0.25	-0.09	0.01	0.09
NaD	0.16	0.20	0.19	0.11	-0.06	0.25
[Cu(Pip)(NaD)]	-1.58	-2.69	-2.35	-2.64	-1.26	-2.14
[Co(Pip)(NaD)]	-2.00	-3.00	-2.78	-3.04	-1.59	-2.58

The physicochemical parameters predicted for both the ligands, Pip and NaD and their metal complexes are presented (Table 7). Only the ligand, NaD possesses a molecular weight <500, others are higher especially the complexes due to the coordination with the metal ions and other ligands. They are poorly soluble in water with fair molar refractivity except for NaD which is moderately soluble. This could be traced to the lipophilicity induced by the aromatic rings in the ligand moieties. They have hydrogen bond donor (HBD) groups <5 and hydrogen bond acceptors (HBA) <10 except the ligands. These are favorable pharmacophores for interaction with residues within various biological targets. They display topological polar surface area (TPSA) >60Å standard compared to the parent ligands possibly due to their new structural morphology brought about by coordination.

Table 7: Physicochemical properties of Pip, NaD and their complexes.

Compound	Mol.wt	Fraction Csp3[a]	HBA[b]	HBD[c]	Molar Refractivity	Water Solubility	TPSA[d] (Å^2)
Pip	535.51	0.38	4	0	168.72	Poorly soluble	38.74
NaD	296.15	0.07	2	2	77.55	Moderately soluble	49.33
[Cu(Pip)(NaD)]	893.19	0.28	6	0	246.70	Poorly soluble	68.28
[Co(Pip)(NaD)]	924.61	0.28	8	2	252.79	Poorly soluble	86.74

a: The ratio of sp^3 hybridized carbon over the total number of carbon atoms in a molecule; b: The number of hydrogen bond acceptors; c: The number of hydrogen bond donors; d: Topological polar surface area.

The predicted pharmacokinetic profiles of the ligands and their complexes (Table 8) indicate that the complexes have low ability for gastrointestinal absorption compared to the ligand and none of them can predictably penetrate the blood-brain barrier (BBB), inhibit the cytochrome P450, indicating their insignificance for drug-drug interaction to induce adverse effects. We observed that the NaD as a ligand on its own virtually displays expression for CYP1A2 as a sign of possible side effects, and this has been mitigated upon coordination to metal ions, further suggesting less side effect of the metal complexes. They all possess low skin permeation indicated by Log Kp value of -4.47 to -5.56 cm/s and are P-G substrates except the ligand Pip and Cu(II) complex. Although some of them show slight violations to Lipinski's Rule of 5 for drugability (40) due to higher molecular weights than 500 g/mol, commonly to coordination compounds (17,18), however, they demonstrate good pharmacokinetics

and bioavailability amenable for further bioactivity probes.

Table 8: Pharmacokinetics and toxicological properties of Pip, NaD, and their complexes.

Compound	GI Abs.	BBB Permeation	P-G Substrate	CYP1A2 Inhibitor	Log Kp (cm/s)
Pip	High	Yes	Yes	No	-5.56
NaD	High	Yes	No	Yes	-5.14
[Cu(Pip)(NaD)]	Low	No	Yes	No	-4.47
[Co(Pip)(NaD)]	Low	No	No	No	-5.34

Antioxidant Assay

The generation of free radicals in the body often results in inflammation and some other ailments including heart diseases and cancer (15). Therefore, a bioactive agent with the ability to scavenge the generated free radicals in a biological system is advantageously preferred for therapeutic applications. The result of antioxidant studies of the synthesized metal complexes in comparison with ascorbic acid as a standard is contained in Table 9. From the IC_{50} values of 165.09 and 382.7 µg/mL, the synthesized metal complexes demonstrate stronger potentials to scavenge free radicals than ascorbic acid whose IC_{50} value stands at 7526 µg/mL and thus, could be good as antioxidants.

Table 9: Results for the DPPH screening for ascorbic acid and the metal complexes.

Concentration (µg/mL)	[Cu(Pip)(NaD)]		[Co(Pip)(NaD)]		Ascorbic Acid	
	Absorbance	% Inhibition	Absorbance	% Inhibition	Absorbance	% Inhibition
100	0.209±0.167	3308	0.137±0.001	2736.7	0.0074±0.003	87.17
200	0.225±0.218	4348.9	0.159±0.007	3144.8	0.079±0.001	86.31
300	0.270±0.242	4838.8	0.355±0.004	7144.89	0.081±0.003	85.96
400	0.375±0.233	4955	0.345±0.003	6940.81	0.075±0.002	87.00
500	0.336±0.179	5553.1	0.319±0.024	6410.2	0.079±0.001	86.31
IC_{50}	382.7		165.09		7526	

Antibacterial activity

The average zones of inhibitions shown in Figure 6 indicate that the metal complexes exhibit stronger inhibition effects on the test organisms than the parent ligands and in good competition with a renowned antibiotic, ciprofloxacin at all concentrations *in vitro*. It could also be observed that antibacterial potency in each case appears to be concentration-dependent as the degree of inhibition increases with an increase in concentration (41). The complexes inhibit the bacterial growth at similar minimal bactericidal concentration and in strong competition with a renowned antibiotic for treating bacterial resistance, ciprofloxacin. The improved activity of the metal-drug chelates can be justified based on the chelation effect (42) and this indicates the worthiness of the complexes for therapeutic transformational probes against drug-resistant bacterial infections upon further studies.

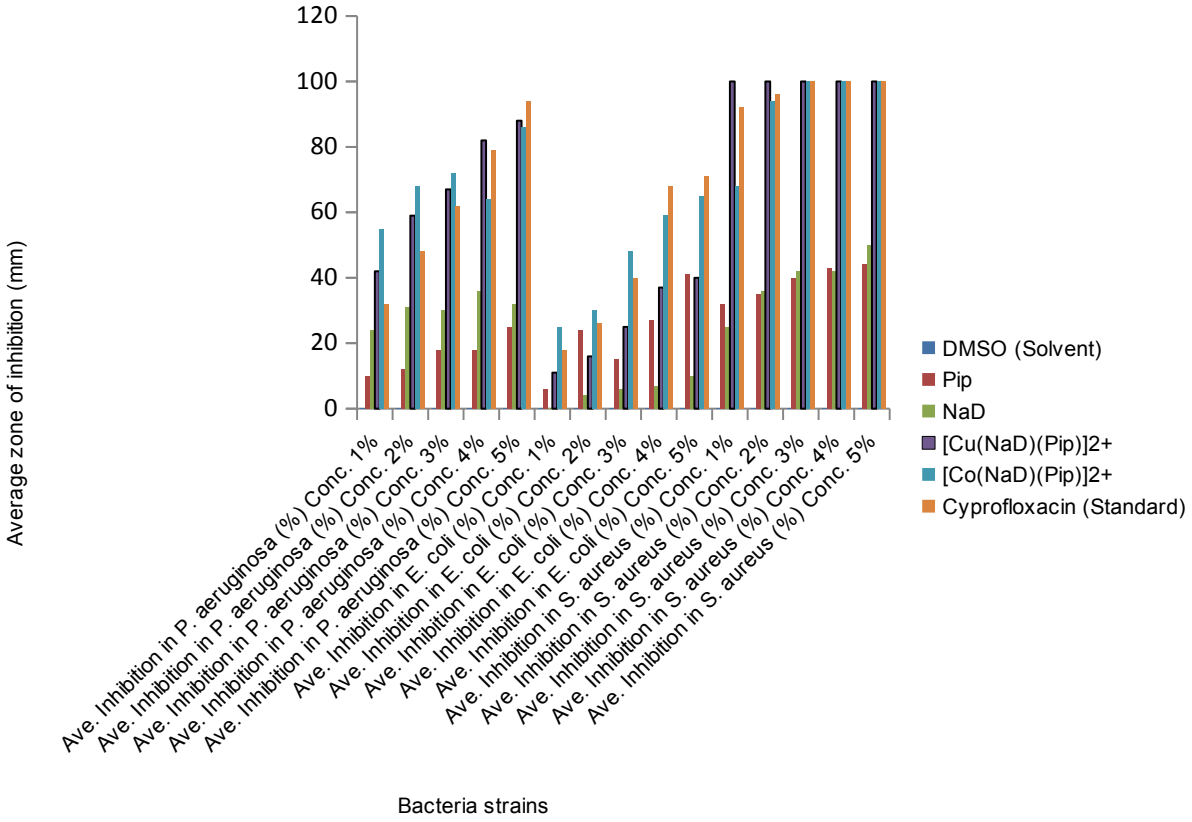


Figure 6: Antibacterial Activities of the ligands, the complexes and the controls.

CONCLUSIONS

Synthesis of coordination compounds consisting of Cu(II), Co(II), piperaquine, and diclofenac have been carried through a reflux mechanism. The characterization results provide succinct evidence of coordination involving the two ligands, piperaquine and diclofenac each as bidentate, through NH, COO and Cl groups, suggesting octahedral geometry, low spin, paramagnetism in both Cu(II) and Co(II) complexes. Powder XRD data reveals the basic morphology of the complexes as polycrystallites consisting of simple, face-centered and body-centered cubes with the overall orthorhombic arrangement but not as single crystals possibly due to the presence of some impurity even after recrystallization. The *in silico* biological studies show that the synthesized complexes possess strong potentials for interaction with various biological targets as therapeutic agents and demonstrate lesser expression for toxicity. The *in vitro* antioxidant and antibacterial assays portray the complexes with higher antioxidant and bactericidal efficacy than the parent ligands and some renowned standards. Although, the limitations in this study include the inability to obtain single crystals of the complexes through which the exact atomic arrangements could be depicted by X-ray crystallography. Further analyses such as the TGA and EPR could provide more accurate information on the coordinated water molecules as well as the suggested paramagnetism, and more robust biological experiments are required for future study. However, the research represents a promising model for novel antioxidant and antibacterial therapeutic designs.

CONFLICT OF INTEREST

The authors declare no conflict of interest in the study.

ACKNOWLEDGEMENT

The authors wish to acknowledge the Tetfund Nigeria for PhD scholarship awarded to YOA.

REFERENCES

1. Naglah AM, Al-Omar MA, Almehizia AA, AlKahtani HM, Bhat MA, Al-Shakliah NS, et al. Synthesis, thermogravimetric, and spectroscopic characterizations of three palladium metal(II) ofloxacin drug and amino acids mixed ligand complexes as advanced antimicrobial materials. Journal of Molecular Structure. 2021 Feb;1225:129102. DOI: https://doi.org/10.1016/j.molstruc.2020.129102.

2. Mohamed GG, El-Sherif AA, Saad MA, El-Sawy SEA, Morgan ShM. Mixed-ligand complex formation of tenoxicam drug with some transition metal ions in

presence of valine: Synthesis, characterization, molecular docking, potentiometric and evaluation of the humeral immune response of calves. Journal of Molecular Liquids. 2016 Nov;223:1311–32. DOI: https://doi.org/10.1016/j.molliq.2016.09.065.

3. Bergamo A, Dyson PJ, Sava G. The mechanism of tumour cell death by metal-based anticancer drugs is not only a matter of DNA interactions. Coordination Chemistry Reviews. 2018 Apr;360:17–33. DOI: https://doi.org/10.1016/j.ccr.2018.01.009.

4. Boros E, Dyson PJ, Gasser G. Classification of Metal-Based Drugs according to Their Mechanisms of Action. Chem. 2020 Jan;6(1):41–60. DOI: https://doi.org/10.1016/j.chempr.2019.10.013.

5. Schmidt C, Karge B, Misgeld R, Prokop A, Franke R, Brönstrup M, et al. Gold(I) NHC Complexes: Antiproliferative Activity, Cellular Uptake, Inhibition of Mammalian and Bacterial Thioredoxin Reductases, and Gram-Positive Directed Antibacterial Effects. Chem Eur J. 2017 Feb 3;23(8):1869–80. DOI: https://doi.org/10.1002/chem.201604512.

6. Zhou G, Shi Q-S, Huang X-M, Xie X-B. The Three Bacterial Lines of Defense against Antimicrobial Agents. IJMS. 2015 Sep 9;16(9):21711–33. DOI: https://doi.org/10.3390/ijms160921711.

7. Paladini F, Pollini M, Sannino A, Ambrosio L. Metal-Based Antibacterial Substrates for Biomedical Applications. Biomacromolecules. 2015 Jul 13;16(7):1873–85. DOI: https://doi.org/10.1021/acs.biomac.5b00773.

8. Alven S, Aderibigbe BA, Balogun MO, Matshe WMR, Ray SS. Polymer-drug conjugates containing antimalarial drugs and antibiotics. Journal of Drug Delivery Science and Technology. 2019 Oct;53:101171. DOI: https://doi.org/10.1016/j.jddst.2019.101171.

9. Turner RJ. Metal-based antimicrobial strategies. Microb Biotechnol. 2017 Sep;10(5):1062–5. DOI: https://doi.org/10.1111/1751-7915.12785.

10. Fiori ATM, Nakahata DH, Cuin A, Lustri WR, Corbi PP. Synthesis, crystallographic studies, high resolution mass spectrometric analyses and antibacterial assays of silver(I) complexes with sulfisoxazole and sulfadimethoxine. Polyhedron. 2017 Jan;121:172–9. DOI: https://doi.org/10.1016/j.poly.2016.09.046.

11. Divya K, Narayana B, Samshuddin S. New spectrophotometric methods for the determination of sulfadoxine by the formation of Co(II) complexes. Journal of Saudi Chemical Society. 2016 Sep;20:S536–40. DOI: https://doi.org/10.1016/j.jscs.2013.03.011.

12. K. O. Ogunniran. Cu(II) and Fe(III) complexes of sulphadoxine mixed with pyramethamine: Synthesis, characterization, antimicrobial and toxicology study. Int J Phys Sci [Internet]. 2012 Mar 23 [cited 2021 May 3];7(13). Available from: http://www.academicjournals.org/IJPS/abstracts/abstracts/abstract2012/23Mar/Ogunniran%20et%20al.htm

13. Hu Y-Q, Gao C, Zhang S, Xu L, Xu Z, Feng L-S, et al. Quinoline hybrids and their antiplasmodial and antimalarial activities. European Journal of Medicinal Chemistry. 2017 Oct;139:22–47. DOI: https://doi.org/10.1016/j.ejmech.2017.07.061.

14. Idemudia O, Sadimenko A, Hosten E. Metal Complexes of New Bioactive Pyrazolone Phenylhydrazones; Crystal Structure of 4-Acetyl-3-methyl-1-phenyl-2-pyrazoline-5-one phenylhydrazone Ampp-Ph. IJMS. 2016 May 18;17(5):687. DOI: https://doi.org/10.3390/ijms17050687.

15. Kakoulidou C, Gritzapis PS, Hatzidimitriou AG, Fylaktakidou KC, Psomas G. Zn(II) complexes of (E)-4-(2-(pyridin-2-ylmethylene)hydrazinyl)quinazoline in combination with non-steroidal anti-inflammatory drug sodium diclofenac: Structure, DNA binding and photo-cleavage studies, antioxidant activity and interaction with albumin. Journal of Inorganic Biochemistry. 2020 Oct;211:111194. DOI: https://doi.org/10.1016/j.jinorgbio.2020.111194.

16. Ayipo YO, Obaleye JA, Badeggi UM. Novel metal complexes of mixed piperaquine-acetaminophen and piperaquine-acetylsalicylic acid: Synthesis, characterization and antimicrobial activities. Journal of the Turkish Chemical Society, Section A: Chemistry. 2016 Nov 11;4(1):313–313. DOI: https://doi.org/10.18596/jotcsa.287331.

17. Okasha RM, AL-Shaikh NE, Aljohani FS, Naqvi A, Ismail EH. Design of Novel Oligomeric Mixed Ligand Complexes: Preparation, Biological Applications and the First Example of Their Nanosized Scale. IJMS. 2019 Feb 10;20(3):743. DOI: https://doi.org/10.3390/ijms20030743.

18. Syed Ali Fathima S, Paulpandiyan R, Nagarajan ER. Expatiating biological excellence of aminoantipyrine derived novel metal complexes: Combined DNA interaction, antimicrobial, free radical scavenging studies and molecular docking simulations. Journal of Molecular Structure. 2019 Feb;1178:179–91. DOI: https://doi.org/10.1016/j.molstruc.2018.10.021.

19. Bunaciu AA, Udriştioiu E gabriela, Aboul-Enein HY. X-Ray Diffraction: Instrumentation and Applications. Critical Reviews in Analytical Chemistry. 2015 Oct 2;45(4):289–99. DOI: https://doi.org/10.1080/10408347.2014.949616.

20. Dorset DL. Crystal Structure Analysis. In: Structural Electron Crystallography [Internet]. Boston, MA: Springer US; 1995 [cited 2021 May 3]. p. 95–133. Available from: http://link.springer.com/10.1007/978-1-4757-6621-9_4.

21. Holder CF, Schaak RE. Tutorial on Powder X-ray Diffraction for Characterizing Nanoscale Materials. ACS Nano. 2019 Jul 23;13(7):7359–65. DOI: https://doi.org/10.1021/acsnano.9b05157.

22. Daina A, Michielin O, Zoete V. SwissADME: a free web tool to evaluate pharmacokinetics, drug-likeness and medicinal chemistry friendliness of small molecules. Sci Rep. 2017 May;7(1):42717. DOI: https://doi.org/10.1038/srep42717.

23. Limbago B. M100-S11, Performance standards for antimicrobial susceptibility testing. Clinical Microbiology Newsletter. 2001 Mar;23(6):49. DOI: https://doi.org/10.1016/S0196-4399(01)88009-0.

24. Nichols L. 6.1C: Melting Point Theory [Internet]. Chemistry LibreTexts; 2020. Available from: https://chem.libretexts.org/Bookshelves/Organic_Chemistry/Book%3A_Organic_Chemistry_Lab_Techniques_(Nichols)/06%3A_Miscellaneous_Techniques/6.01%3A_Melting_Point/6.1C%3A__Melting_Point_Theory

25. Refat MS, Mohamed GG, Ibrahim MYS, Killa HMA, Fetooh H. Synthesis and Characterization of Coordination Behavior of Diclofenac Sodium Drug Toward Hg(II), Pb(II), and Sn(II) Metal Ions: Chelation Effect on Their Thermal Stability and Biological Activity. Synthesis and Reactivity in Inorganic, Metal-Organic, and Nano-Metal Chemistry. 2014 Feb 7;44(2):161–70. https://doi.org/10.1080/15533174.2012.752009.

26. Perontsis S, Dimitriou A, Fotiadou P, Hatzidimitriou AG, Papadopoulos AN, Psomas G. Cobalt(II) complexes with the non-steroidal anti-inflammatory drug diclofenac and nitrogen-donor ligands. Journal of Inorganic Biochemistry. 2019 Jul;196:110688. DOI: https://doi.org/10.1016/j.jinorgbio.2019.04.002.

27. Osunniran W, Obaleye J, Ayipo Y, Rajee A, Enemose E. Six Coordinate Transition Metal (II) Complexes of Mixed Ligands of Eflornithine Hydrochloride Hydrate and 2,2-Bipyridine: Synthesis, Characterization and Antibacterial Study. Jordan J Chem. 2018;13(3):149–57. URL: http://jjc.yu.edu.jo/index.php/jjc/article/view/39.

28. Al-Adilee K, Dakheel H. Synthesis, Spectral and Biological Studies of Ni(II), Pd(II), and Pt(IV) Complexes with New Heterocyclic ligand Derived from Azo-Schiff Bases Dye. Eurasian J Anal Chem [Internet]. 2018 Oct 2 [cited 2021 May 3];13(6). Available from: http://www.journalssystem.com/ejac/,97267,0,2.html

29. Lakshmi S, Endo T, Siva G. Electronic (Absorption) Spectra of 3d Transition Metal Complexes. In: Akhyar Farrukh M, editor. Advanced Aspects of Spectroscopy [Internet]. InTech; 2012 [cited 2021 May 3]. Available from: http://www.intechopen.com/books/advanced-aspects-of-spectroscopy/electronic-absorption-spectra-of-3d-transition-metal-complexes

30. Radoń M, Rejmak P, Fitta M, Bałanda M, Szklarzewicz J. How can [Mo IV (CN) 6] 2− , an apparently octahedral (d) 2 complex, be diamagnetic? Insights from quantum chemical calculations and magnetic susceptibility measurements. Phys Chem Chem Phys. 2015;17(22):14890–902. DOI: https://doi.org/10.1039/C4CP04863F.

31. Salazar-Medina AJ, Gámez-Corrales R, Ramírez JZ, González-Aguilar GA, Velázquez-Contreras EF. Characterization of metal-bound water in bioactive Fe(III)-cyclophane complexes. Journal of Molecular Structure. 2018 Feb;1154:225–31. DOI: https://doi.org/10.1016/j.molstruc.2017.10.018.

32. Xu X-H, Kuang M-Q. Interpretation of the Electron Paramagnetic Resonance Spectra of Copper(II)–Tyrosine Complex. Zeitschrift für Naturforschung A. 2017 Dec 20;73(1):75–8. DOI: https://doi.org/10.1515/zna-2017-0239.

33. Ott JC, Wadepohl H, Enders M, Gade LH. Taking Solution Proton NMR to Its Extreme: Prediction and Detection of a Hydride Resonance in an Intermediate-Spin Iron Complex. J Am Chem Soc. 2018 Dec 19;140(50):17413–7. DOI: https://doi.org/10.1021/jacs.8b11330.

34. Müntener T, Böhm R, Atz K, Häussinger D, Hiller S. NMR pseudocontact shifts in a symmetric protein homotrimer. J Biomol NMR. 2020 Sep;74(8–9):413–9. DOI: https://doi.org/10.1007/s10858-020-00329-7.

35. Ramotowska S, Wysocka M, Brzeski J, Chylewska A, Makowski M. A comprehensive approach to the analysis of antibiotic-metal complexes. TrAC Trends in Analytical Chemistry. 2020 Feb;123:115771. DOI: https://doi.org/10.1016/j.trac.2019.115771.

36. Speakman S. Basics of X-Ray Powder Diffraction [Internet]. MIT; 2018. Available from: http://prism.mit.edu/xray.

37. Wang Q, Huang YM, Ma XL, Li SS, Li H. X-ray powder diffraction data for piperaquine, C 29 H 32 Cl 2 N 6. Powder Diffr. 2015 Sep;30(3):289–92. DOI: https://doi.org/10.1017/S0885715615000524.

38. Ibragimov A, Ashurov J, Dusmatov A, Ibragimov A. Crystal structure and Hirshfeld surface analysis of the orthorhombic polymorph of a Zn II complex with 3,5-dinitrobenzoic acid and ethylenediamine. Acta Crystallogr E Cryst Commun. 2020 Jul 1;76(7):1113–6. DOI: https://doi.org/10.1107/S2056989020007938.

39. Marino SF, Regan L. Secondary ligands enhance affinity at a designed metal-binding site. Chemistry & Biology. 1999 Sep;6(9):649–55. DOI: https://doi.org/10.1016/S1074-5521(99)80116-1.

40. Lipinski CA. Lead- and drug-like compounds: the rule-of-five revolution. Drug Discovery Today: Technologies. 2004 Dec;1(4):337–41. DOI: https://doi.org/10.1016/j.ddtec.2004.11.007.

41. Kuti JL. OPTIMIZING ANTIMICROBIAL PHARMACODYNAMICS: A GUIDE FOR YOUR STEWARDSHIP PROGRAM. Revista Médica Clínica Las Condes. 2016 Sep;27(5):615–24. DOI: https://doi.org/10.1016/j.rmclc.2016.08.001.

42. Coraça-Huber DC, Dichtl S, Steixner S, Nogler M, Weiss G. Iron chelation destabilizes bacterial biofilms and potentiates the antimicrobial activity of antibiotics against coagulase-negative Staphylococci. Pathogens and Disease [Internet]. 2018 Jul 1 [cited 2021 May 3];76(5). Available from: https://academic.oup.com/femspd/article/doi/10.1093/femspd/fty052/5026171.